X.S. Rozhkova[1]*, A.K. Aimukhanov[1], B.R. Ilyassov[2], A.K. Tussupbekova[1],
A.K. Zeinidenov[1], A.M. Alexeev[1,3], A.M. Zhakanova[1]

[1]Buketov University, Scientific Center for Nanotechnology and Functional Nanomaterials, Karaganda, Kazakhstan;
[2]Astana IT University, Astana, Kazakhstan;
[3]Kazan Federal University, Kazan, Russia
(*E-mail: ksusharogovaya@mail.ru)

Effect of WS2 nanoparticles on the current-voltage characteristics of a polymer solar cell

The paper presents the results of studies of the effect of tungsten disulfide nanoparticles on the optical and electrotransport characteristics of PEDOT: PSS thin films in polymer solar cells. Tungsten disulfide (WS2) nanoparticles were obtained by laser ablation in isopropyl alcohol. The average size of nanoparticles were determined by dynamic light scattering and is ~38 nm. The concentration of WS2 nanoparticles in the solution was calculated based on the density of the WS2 substance. The absorption spectrum of nanoparticles in isopropyl alcohol has been measured. Two bands are observed in 500-900 nm regions, which are associated with direct exciton transitions A1 and B1 in two-dimensional transition metal dichalcogenides with 2H phase. WS2 nanoparticles were added in PEDOT: PSS solution and thin films were deposited from the prepared solution by spin-coating. PEDOT: PSS thin films doped with WS2 were studied by atomic force microscopy (AFM). The arithmetic mean deviation of the surface roughness (R_a) was estimated. Doping with WS2 nanoparticles leads to the increase in R_a of PEDOT: PSS thin films. The optical absorption spectra of doped films have been measured. Also, doping PEDOT: PSS with WS2 nanoparticles results in a long-wavelength shift of the PEDOT absorption maximum. The optimal concentration of WS2 nanoparticles for the preparation of doped PEDOT: PSS thin films is determined, at which the film resistance decreases by almost 2 times, the recombination resistance of charge carriers increases by 4.7 times, and the efficiency of the polymer solar cell increases to 1.94 %.

Keywords: PEDOT: PSS, WS2 nanoparticles, hole-transport layer, surface morphology, absorption spectra, impedance spectroscopy, organic solar cell, volt-ampere characteristics.

Introduction

In the last decade, organic solar cells (OSCs) have been widely developed due to their low cost, ease of fabrication, technology flexibility, large-scale production, and wide choice of materials. The power conversion efficiency of OSCs has now exceeded 18 % [1-4]. The boost of OSCs performance is attributed to the development of new materials for photoactive layers and due to the optimization of the film morphology [5-9]. However, the characteristics of a hole-transport layer, which extracts holes from the photoactive layer and deliver them to external electrodes, plays an important role in improving the PCE of the OSC [10-15].

Among hole-transport materials, the conjugated polymer poly(3,4-ethylenedioxythiophene): poly(4-styrenesulfonate) (PEDOT: PSS) is the most widely used hole-transport layer (HTL) in OSCs due to its excellent water solubility and high conductivity [16]. The analysis of previous works has shown that the reason for the low performance of organic solar cells with a PEDOT: PSS HTL is the presence of defects at the interface with the photoactive layer. As results, poor hole injection and severe recombination processes occurs in OCSs. To solve this problem, researchers have proposed various methods for modifying and introducing additives into PEDOT: PSS [17-24].

Two-dimensional transition metal dichalcogenides are used as such additives. They have attracted the attention of researchers due to their adjustable band gap and high carrier mobility [25, 26]. Due to the special single layer structure of WS2, unshared pairs of electrons of the S atom can carry out fast transport, thereby increasing the mobility of charge carriers [3, 27]. These advantages allow us to consider them as promising materials for composite photovoltaic cells [28-31].

In this work, we have developed a completely new highly efficient composite hole-transport layer: PEDOT: PSS: NP WS2. doped with WS2 nanoparticles, which increased the efficiency of the organic solar cell by 1.8 times.

Experimental

The following materials were used in this work: PEDOT: PSS (1 %, Ossila Al4083), WS_2 (pure > 99 %, Borun Chemicals), P3HT (pure 97.6 %, Ossila), PC61BM (pure > 99 %, Ossila). The structural formulas of the chemicals are shown in Figure 1. The cleaning of the substrates was carried out according to the procedure described in [32]. Nanoparticles were fabricated by laser ablation of the WS_2 in Isopropanol. Nd: YAG solid-state laser (SOLAR LQ 529, λ_{gen} =532 nm, E_{pulse} =180 mJ, τ=20 ns) was used for the ablation. Ablation time ranged from 15 to 30 minutes.

Before the film deposition, the PEDOT: PSS solution was filtered through a 0.45 micrometer filter. Then nanoparticles were added to the PEDOT: PSS solution at various concentrations: from 2 % to 10 %. PEDOT: PSS: NP WS_2 nanocomposite films were spin-coated on the surface of FTO substrates (by SPIN150i spin-coater manufactured by Semiconductor Production System) at a rotation speed of 5000 rpm. After, the films were annealed at a temperature of 120 °C for 10 minutes to complete the solvent evaporation and improve film crystallinity.
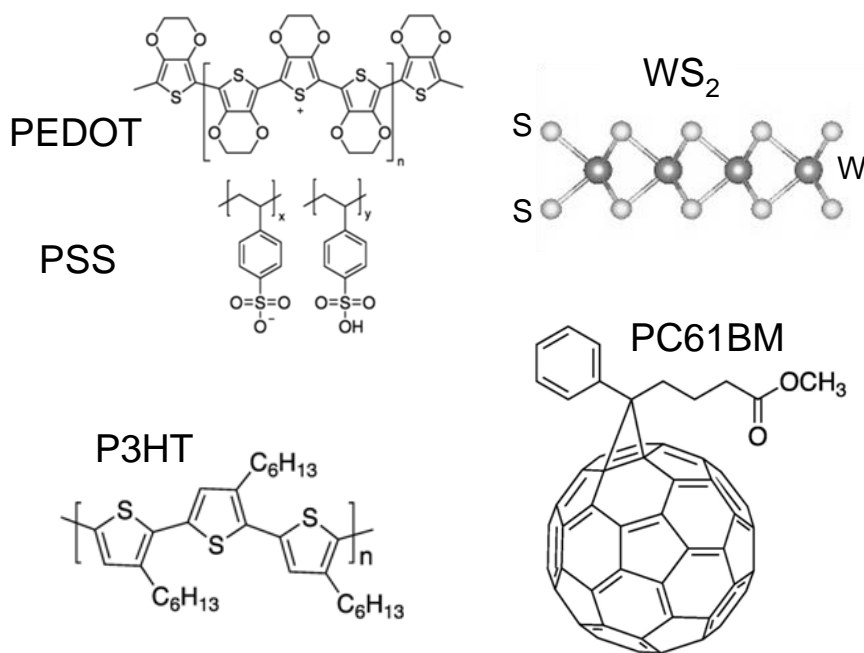
Figure 1. Structural formulas of PEDOT: PSS, WS_2, P3HT and PC61BM

As a photoactive layer of OSCs a mixture of P3HT: PC61BM with a ratio of 1:0.6 was used as a donor and acceptor material, respectively. The mixture was prepared as follows: P3HT (~15.6 mg) and PC61BM (~9.4 mg) were dissolved in 1 ml of chlorobenzene and the solution was stirred at 60 °C for 24 hours. The prepared solution was filtered through a 0.45 micrometer filter, and then deposited on the surface of PEDOT: PSS: NP WS_2/FTO/glass by spin-coating at a rotation speed of 2000 rpm. Next, the photoactive layer was subjected to thermal annealing at 120 °C for 10 minutes to improve the crystallinity of the film. Finally, aluminum electrodes with a thickness of 100 nm were deposited in a vacuum of 10^5 Torr by thermal evaporation using the CY-1700x-spc-2 evaporator (Zhengzhou CY Scientific Instruments Co., Ltd).

The surface topography of the samples was studied using the JSPM-5400 atomic force microscope (JEOL Ltd, Japan) and the Tescan Mira 3 electron microscope. The surface morphology parameters were calculated using the Winspm II Data Processing software package (JEOL Ltd). The size distribution of nanoparticles in isopropanol was determined by using the Zetasizer Nano ZS. The optical characteristics of the solution with nanoparticles and nanocomposite films were studied using the Avantes AvaSpec-ULS2048CL-EVO spectrometer. A combined deuterium-halogen AvaLight-DHc light source with an operating range of 200-2500nm was used as a radiation source. Measurements of the impedance spectra were carried out on a potentiostat-galvanostat P45X in the impedance mode. The spectra were fitted using the EIS-analyzer software package, and the experimental data were analyzed using diffusion-recombination models. The I-V

characteristics of OCS cells were determined by the Sol3A Class AAA Solar Simulators (Newport) with PVIV-1A I-V Test Station.

Results and Discussion

Figure 2a shows the SEM image of WS₂ nanoparticles deposited on the surface of quartz glass. It can be seen from the Figure 2a that the nanoparticles have a round shape, their diameter varies from 10 to 50 nm. Figure 2b shows the absorption spectrum of WS₂ nanoparticles in isopropyl alcohol. The figure shows that two characteristic absorption peaks in the 500-900 nm region are clearly observed, which correspond to direct exciton transitions A1 and B1 in TMDC with the 2H phase [33-36].

The inset of Figure 2b shows the size distribution of WS₂ nanoparticles in an isopropyl alcohol solution. As can be seen from the diagram, the average size of nanoparticles in solution is 38 nm.

| a | b |
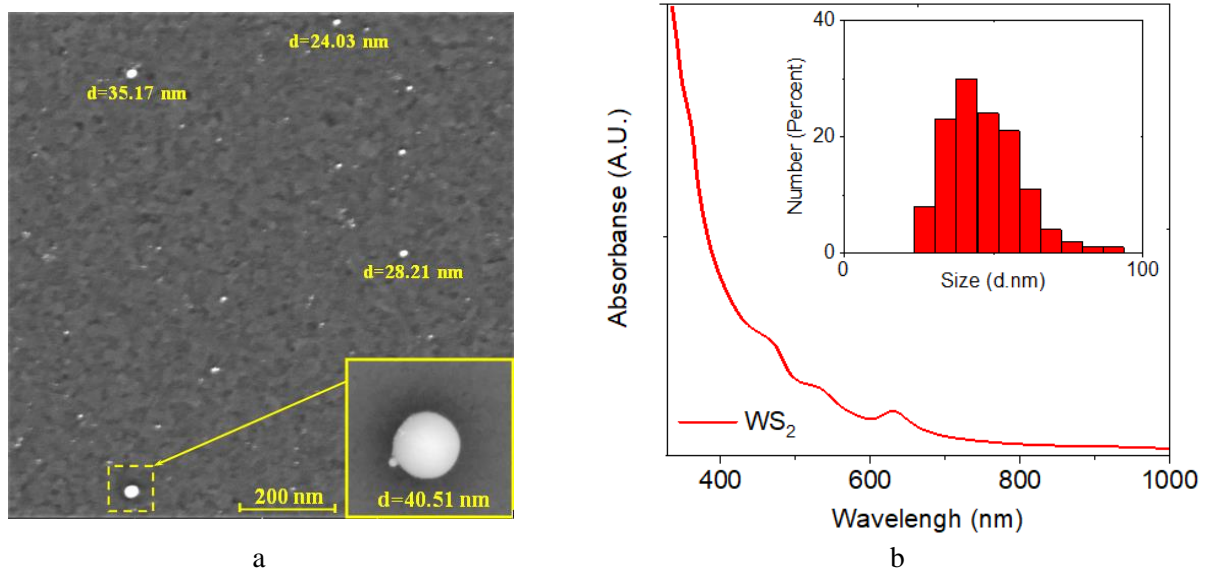
Figure 2. SEM image of WS₂ nanoparticles (a) and the absorption spectrum of WS₂ nanoparticles in isopropanol solution (b). In the insert, the size distribution of WS₂ nanoparticles in isopropanol solution

To fabricate nanocomposite films, WS₂ nanoparticles were added to a PEDOT: PSS solution. The concentration of WS₂ nanoparticles in the solution was calculated based on the density of WS₂ according to the formula:

$$C_{NP} = \frac{C_{WS_2}}{m_{NP} \cdot N_A} = \frac{C_{WS_2}}{\rho_{WS_2} \cdot V_{NP} \cdot N_A} = \frac{\frac{m_{WS_2}}{V_{sol} M_{WS_2}}}{\rho_{WS_2} \cdot \frac{4\pi r^3}{3} \cdot N_A} \left(\frac{mol}{L}\right),$$

where C_{NP} is the concentration of nanoparticles in solution;
C_{WS2} is the concentration of the substance in the solution before laser ablation of the WS₂;
m_{NP} is the weight of the average nanoparticle;
N_A is the Avogadro's number;
ρ_{WS2} is the density of WS₂ substance;
V_{NP} is the volume of the average nanoparticle;
m_{WS2} is the weight of the WS₂ substance;
V_{sol} is the volume of solvent used in laser ablation of the substance;
M_{WS2} is the molar mass of the WS₂ substance;
r is the average radius nanoparticle.

AFM images of the surface morphology of PEDOT: PSS nanocomposite films are shown in Figure 3. They shows that the pristine PEDOT: PSS has a fine-grained structure with the surface roughness (R_a) of 0.54 nm. Doping PEDOT: PSS with WS₂ nanoparticles affects R_a. The increase of the concentration from 0 to 6 % results in the slow growth of R_a from 0.54 nm to 0.58 nm, respectively (Table 1). Further increase of the

concentration up to 10 % results to the sharp growth of Ra reaching a value of 0.75 nm. Table 1 and Figure 4 shows this surface roughness dependence on WS$_2$ nanoparticles concentration.

PEDOT: PSS   PEDOT: PSS: WS$_2$ 10µl (2 %)   PEDOT: PSS: WS$_2$ 20µl (4 %)

PEDOT: PSS: WS$_2$ 30µl (6 %)   PEDOT: PSS: WS$_2$ 40µl (8 %)   PEDOT: PSS: WS$_2$ 50µl (10 %)
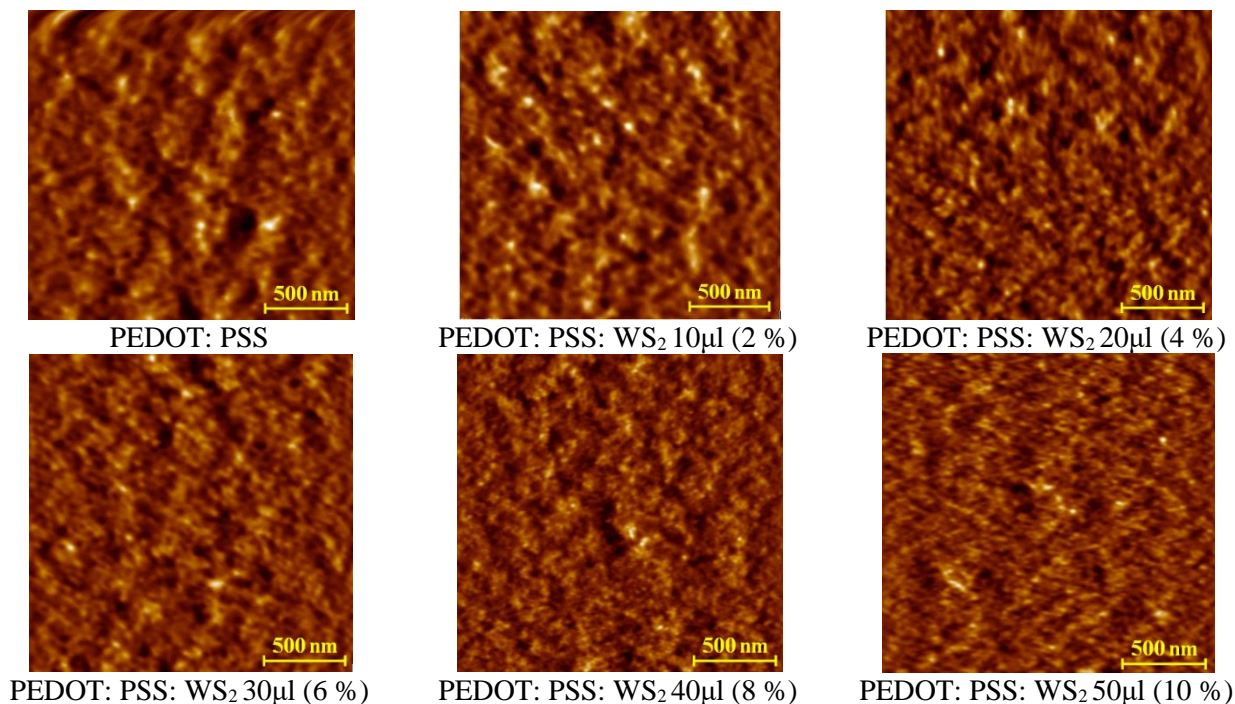
Figure 3. AFM images of PEDOT: PSS: WS$_2$ nanocomposite films with different concentrations of nanoparticles in solution

Table 1

The dependence of surface roughness WS$_2$ doped PEDOT: PSS thin films on WS$_2$ nanoparticles concentration

Sample	R_a, nm	C_{NP}, mol/L
PEDOT: PSS	0.54	0
PEDOT: PSS: WS$_2$ 10µl (2 %)	0.56	$0.47 \cdot 10^{-13}$
PEDOT: PSS: WS$_2$ 20µl (4 %)	0.57	$0.94 \cdot 10^{-13}$
PEDOT: PSS: WS$_2$ 30µl (6 %)	0.58	$1.34 \cdot 10^{-13}$
PEDOT: PSS: WS$_2$ 40µl (8 %)	0.74	$1.87 \cdot 10^{-13}$
PEDOT: PSS: WS$_2$ 50µl (10 %)	0.75	$2.34 \cdot 10^{-13}$
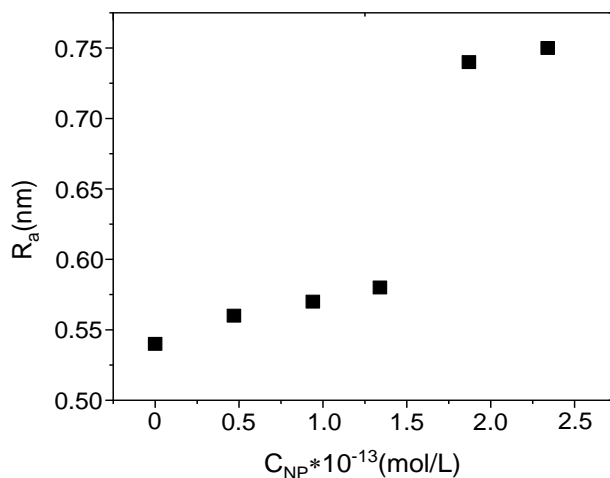
Figure 4. Diagram of dependence of film surface roughness on concentration of WS$_2$ nanoparticles in PEDOT: PSS polymer solution

Figure 5 shows the absorption spectra of PEDOT: PSS films. It can be seen from the Figure 5 that the PEDOT: PSS film has a maximum at a wavelength of $\lambda_1 = 234.6$ nm related to the absorption of PEDOT and a maximum at 278.2 nm associated with the absorption of the aromatic fragment of PSS [20, 21, 37]. When WS₂ nanoparticles are added to the PEDOT: PSS solution, the optical density decreases and a slight bathochromic shift of the PEDOT absorption maximum is observed. The observed long-wavelength shift of the PEDOT: PSS absorption maximum is associated with a change in the film structure due to the incorporation of WS₂ nanoparticles between the PEDOT and PSS chains [3, 21].
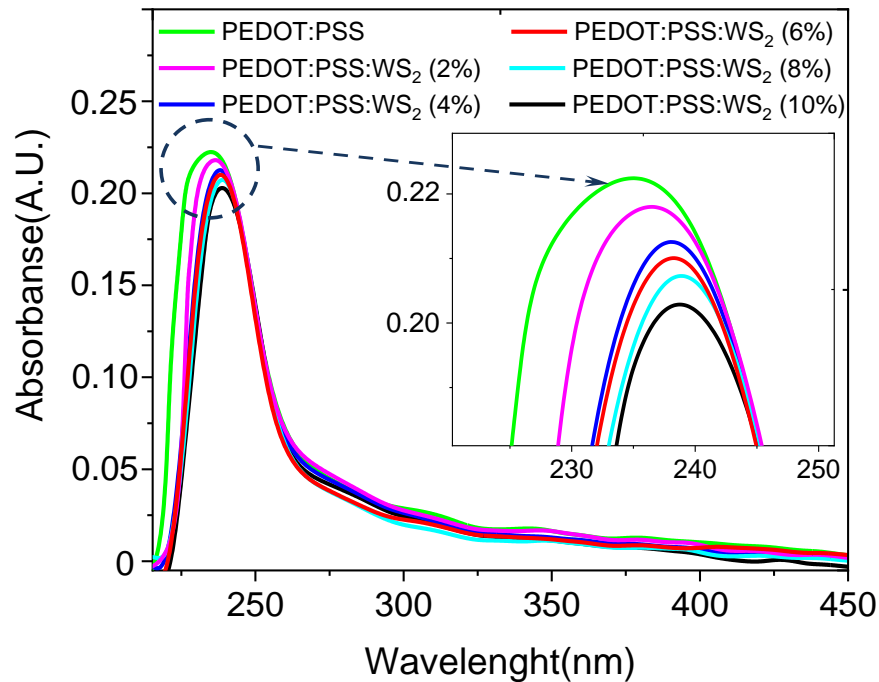
Figure 5. Absorption spectra of PEDOT: PSS: WS₂ nanocomposite films

T a b l e   2

Spectral characteristics of PEDOT: PSS: WS₂ nanocomposite films

Sample	λ_1, nm	λ_2, nm
PEDOT: PSS	234.6	278.2
PEDOT: PSS: WS₂ (2 %)	236.5	278.2
PEDOT: PSS: WS₂ (4 %)	237.9	278.2
PEDOT: PSS: WS₂ (6 %)	238.0	278.2
PEDOT: PSS: WS₂ (8 %)	238.4	278.2
PEDOT: PSS: WS₂ (10 %)	238.9	278.2

The impedance spectra were measured to study the effect of WS₂ nanoparticles on electrotransport properties of the doped PEDOT: PSS film (Fig. 6). The fitting of the impedance spectra was carried out according to the diffusion-recombination model [38].
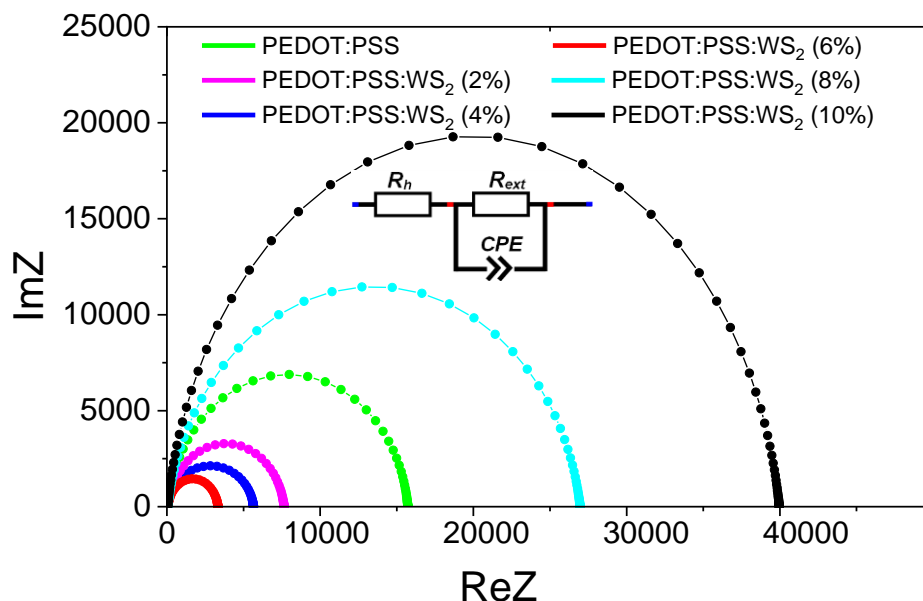
Figure 6. Effect of WS$_2$ nanoparticles on the impedance spectra of the PEDOT: PSS film

The electric transport characteristics were determined from the impedance spectra. The equivalent electrical circuit (Fig. 6) was used to fit impedance spectra. The Table 3 shows the main electrical transport characteristics of the PEDOT: PSS films, where: k_{eff} is the effective charge carrier extraction rate from PEDOT: PSS, τ_{eff} is the effective transit time through PEDOT: PSS layer, R_h is the PEDOT: PSS resistance film, R_{ext} is the transfer resistance of charge carriers at the PEDOT: PSS/electrode interface associated with the extraction of charge carriers from PEDOT: PSS.

Table 3

Effect of WS$_2$ nanoparticles on the electrotransport characteristics of a PEDOT: PSS film

Sample	R_h, Ω	R_{ext}, Ω	k_{eff}, s^{-1}	τ_{eff}, ms
PEDOT: PSS	71.923	15014	75.84	0.013
PEDOT: PSS: WS$_2$ (2 %)	61.51	7322.2	159.09	0.006
PEDOT: PSS: WS$_2$ (4 %)	59.33	5490.4	190.51	0.005
PEDOT: PSS: WS$_2$ (6 %)	45.3	3210.1	398.43	0.003
PEDOT: PSS: WS$_2$ (8 %)	69.547	25856	36.31	0.027
PEDOT: PSS: WS$_2$ (10 %)	63.633	38709	17.15	0.058

Next, PEDOT: PSS: NP WS$_2$ nanocomposite films were used as hole selective electrodes for organic solar cells based on the P3HT: PC61BM photoactive layer (Fig. 7a). The current-voltage curves of the fabricated organic cells are shown in Figure 7b.
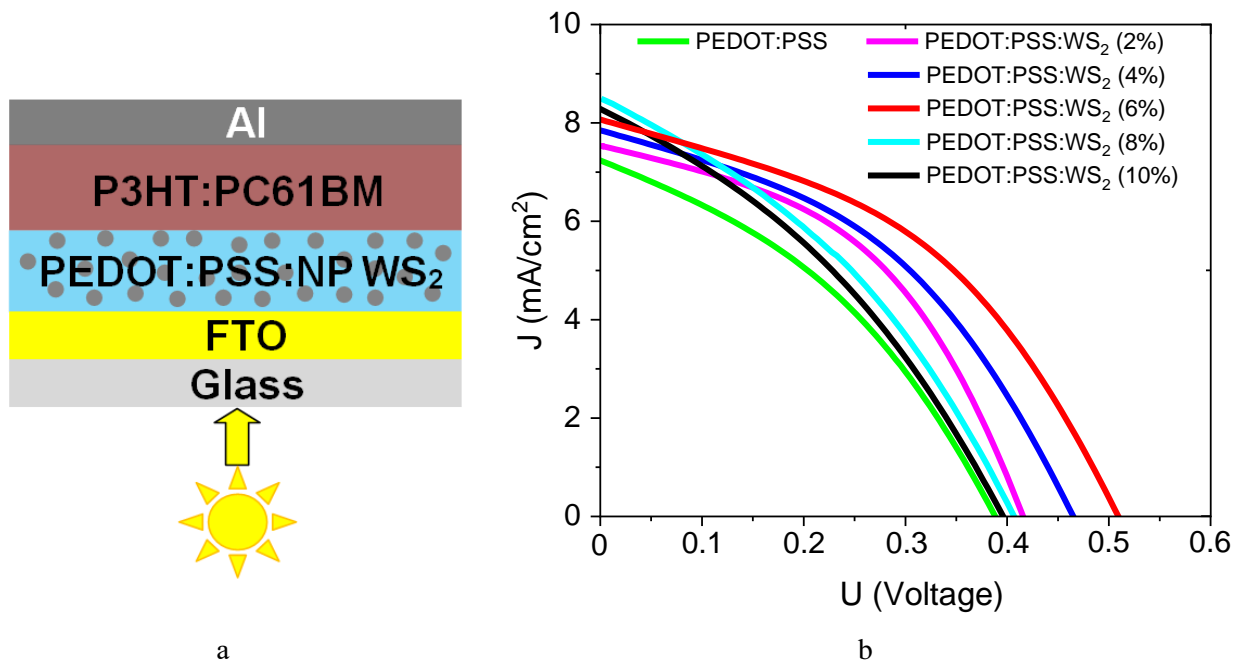
Figure 7. Structure (a) and current-voltage characteristics (b) of an organic solar cell with FTO/PEDOT: PSS: NP WS₂/P3HT: PC61BM/Al architecture.

Table 4 shows the photovoltaic performance of organic solar cells. All OSCs based on PEDOT: PSS doped with WS₂ nanoparticles showed improved J_{sc} and PCE compared to the cell with pristine PEDOT: PSS. OSCs with 6 % WS₂ doped PEDOT: PSS revealed the best performance. In comparison with the device based on pristine PEDOT: PSS, J_{sc}, V_{oc}, FF, and PCE of 6 % WS₂ doped PEDOT: PSS based device increased from 7.20 mA/cm² to 8.06 mA/cm², form 0.39 V to 0.49 V, from 0.37 to 0.49, and from 1.04 % to 1.94 %, respectively. This result indicates that the PEDOT: PSS hole-transport layer doped with WS₂ nanoparticles can block electrons more efficiently, which is an advantage for a higher FF value [3, 39, 40]. In addition, according to the impedance spectra, PEDOT: PSS with WS₂ nanoparticles provides faster injection and transport of holes to the external electrode (FTO), which reduces the probability of hole recombination with PC61BM and improve the efficiency of hole accumulation by the external electrode. However, at higher concentrations of WS₂ nanoparticles (8 % and 10 %) in PEDOT: PSS, a deterioration of the I-V parameters of the OCSs is observed, which is associated with high surface roughness of doped PEDOT: PSS.

Ta b l e 4

I-V characteristics of organic solar cells

Sample	J_{sc}, (mA/cm²)	J_{max}, (mA/cm²)	U_{oc}, (V)	U_{max}, (V)	Fill Factor	Efficiency, %
PEDOT: PSS	7.20	4.50	0.39	0.23	0.37	1.04
PEDOT: PSS: WS₂ (2 %)	7.56	5.31	0.42	0.27	0.45	1.43
PEDOT: PSS: WS₂ (4 %)	7.92	5.64	0.46	0.29	0.45	1.64
PEDOT: PSS: WS₂ (6 %)	8.06	6.25	0.49	0.31	0.49	1.94
PEDOT: PSS: WS₂ (8 %)	8.51	5.21	0.41	0.24	0.36	1.25
PEDOT: PSS: WS₂ (10 %)	8.24	4.96	0.40	0.23	0.35	1.14

Conclusion

As a result of study, it was found that moderate doping PEDOT: PSS with WS₂ nanoparticles leads to an increase in the efficiency of organic solar cells. WS₂ nanoparticles were obtained by laser ablation of the WS₂

in isopropyl alcohol. The average size of WS_2 nanoparticles was 38 nm. It has been shown that the addition of WS_2 nanoparticles to PEDOT: PSS affects the absorption spectra of nanocomposite films. It was found that when WS_2 nanoparticles are added to PEDOT: PSS, a bathochromic shift of the PEDOT absorption maximum is observed, which is associated with a change in the film structure due to the incorporation of WS_2 nanoparticles between the PEDOT and PSS chains. The optimal concentration of WS_2 nanoparticles in the PEDOT: PSS: NP WS_2 nanocomposite film was determined, which is 6 %. At this concentration, the resistance of the nanocomposite film decreases by almost 2 times, and the recombination resistance of charge carriers increases by 4.7 times. OSCs based on 6 % WS_2 doped PEDOT: PSS doped with showed the best performance with PCE of 1.94 %.

References

1   Liu, Q., Jiang, Y., Jin, K., Qin, J., Xu, J., Li, W., Xiong, J., Liu, J., Xiao, Z., Sun, K., Yang, S., Zhang, X., & Ding, L. (2020). 18 % Efficiency organic solar cells, *Science Bulletin*, 65(4), 272-275. https://doi.org/10.1016/j.scib.2020.01.001.

2   Zhang, M., Zhu, L., Zhou, G., Hao, T., Qiu, C., Zhao, Z., Hu, Q., Larson, B.W., Zhu, H., Ma, Z., Tang, Z., Feng, W., Zhang, Y., Russell, T.P., & F. Liu. (2021). Single-layered organic photovoltaics with double cascading charge transport pathways: 18 % efficiencies, *Nature Communications*, 12, 309. https://doi.org/10.1038/s41467-020-20580-8.

3   Wang, Y., Li, N., Cui, M., Li, Y., Tian, X., Xu, X., Rong, Q., Yuan, D., Zhou, G., & Nian, L. (2021). High-performance hole transport layer based on WS_2 doped PEDOT: PSS for organic solar cells, *Organic Electronics*, 99, 106305. https://doi.org/10.1016/j.orgel.2021.106305.

4   Cui, Y., Yao, H., Zhang, J., Xian, K., Zhang, T., Hong, L., Wang, Y., Xu, Y., Ma, K., An, C., He, C., Wei, Z., Gao, F., & Hou, J. (2020). Single-junction organic photovoltaic cells with approaching 18 % efficiency, *Advanced Materials*, 32(19), 1908205. https://doi.org/10.1002/adma.201908205.

5   Nian, L., Kan, Y., Gao, K., Zhang, M., Li, N., Zhou, G., Jo, S.B., Shi, X., Lin, F., Rong, Q., Liu, F., Zhou, G., & Jen, A.K.Y. (2020). Approaching 16 % efficiency in all-small-molecule organic solar cells based on ternary strategy with a highly crystalline acceptor, *Joule*, 4(10), 2223-2236. https://doi.org/10.1016/j.joule.2020.08.011.

6   Gao, K., Kan, Y., Chen, X., Liu, F., Kan, B., Nian, L., Wan, X., Chen, Y., Peng, X., Russell, T.P., Cao, Y., & Jen, A.K. (2020). Low-bandgap porphyrins for highly efficient organic solar cells: materials, morphology, and applications, *Advanced Materials*, 32(32), 1906129. https://doi.org/10.1002/adma.201906129.

7   Gao, K., Jo, S.B., Shi, X., Nian, L., Zhang, M., Kan, Y., Lin, F., Kan, B., Xu, B., Rong, Q., Shui, L., Liu, F., Peng, X., Zhou, G., Cao, Y., & Jen, A.K. (2019). Over 12 % efficiency nonfullerene all-small-molecule organic solar cells with sequentially evolved multilength scale morphologies, *Advanced Materials*, 31(12), 1807842. https://doi.org/10.1002/adma.201807842.

8   Zhu, L., Zhang, M., Zhou, G., Hao, T., Xu, J., Wang, J., Qiu, C., Prine, N., Ali, J., Feng, W., Gu, X., Ma, Z., Tang, Z., Zhu, H., Ying, L., Zhang, Y., & Liu, F. (2020). Efficient organic solar cell with 16.88 % efficiency enabled by refined acceptor crystallization and morphology with improved charge transfer and transport properties, *Advanced Energy Materials*, 10(18), 1904234. https://doi.org/10.1002/aenm.201904234.

9   Yuan, J., Zhang, Y., Zhou, L., Zhang, G., Yip, H.-L., Lau, T.-K., Lu, X., Zhu, C., Peng, H., Johnson, P.A., Leclerc, M., Cao, Y., Ulanski, J., Li, Y., & Zou, Y. (2019). Single-junction organic solar cell with over 15 % efficiency using fused-ring acceptor with electron-deficient core, *Joule*, 3(4), 1140-1151. https://doi.org/10.1016/j.joule.2019.01.004.

10   Zheng, Z., Hu, Q., Zhang, S., Zhang, D., Wang, J., Xie, S., Wang, R., Qin, Y., Li, W., Hong, L., Liang, N., Liu, F., Zhang, Y., Wei, Z., Tang, Z., Russell, T.P., Hou, J., & Zhou, H. (2018). A highly efficient non-fullerene organic solar cell with a fill factor over 0.80 enabled by a fine-tuned hole-transporting layer, *Advanced Materials*, 30(34), 1801801. https://doi.org/10.1002/adma.201801801.

11   Duan, L., Sang, B., He, M., Zhang, Y., Hossain, M.A., Rahaman, M.H., Wei, Q., Zou, Y., Uddin, A., & Hoex, B. (2020). Interface modification enabled by atomic layer deposited ultra ultrathin titanium oxide for high-efficiency and semitransparent organic solar cells, *Solar RRL*, 4(12), 2000497. https://doi.org/10.1002/solr.202000497.

12   Song, X., Liu, G., Gao, W., Di, Y., Yang, Y., Li, F., Zhou, S., & Zhang, J. (2021). Manipulation of zinc oxide with zirconium doping for efficient inverted organic solar cells, *Small*, 17(7), 2006387. https://doi.org/10.1002/smll.202006387.

13   Zhou, H., Zhang, Y., Mai, C.K., Seifter, J., Nguyen, T.Q., Bazan, G.C., & Heeger, A.J. (2015). Solution-processed pH-neutral conjugated polyelectrolyte improves interfacial contact in organic solar cells, *ACS Nano*, 9(1), 371-377. https://doi.org/10.1021/nn505378m.

14   Zhou, H., Zhang, Y., Mai, C.K., Collins, S.D., Nguyen, T.Q., Bazan, G.C., & Heeger, A.J. (2014). Conductive conjugated polyelectrolyte as hole-transporting layer for organic bulk heterojunction solar cells, *Advanced Materials*, 26(5), 780-785. https://doi.org/10.1002/adma.201302845.

15   Zilberberg, K., Gharbi, H., Behrendt, A., Trost, S., & Riedl, T. (2012). Low-temperature, solution-processed MoO(x) for efficient and stable organic solar cells, *ACS Applied Materials & Interfaces*, 4(3), 1164-1168. https://doi.org/10.1021/am201825t.

16 Yin, B., Liu, Q., Yang, L., Wu, X., Liu, Z., Hua, Y., Yin, S., & Chen, Y. (2010). Buffer layer of PEDOT: PSS/graphene composite for polymer solar cells, *Journal of Nanoscience and Nanotechnology*, 10(3), 1934-1938. https://doi.org/10.1166/jnn.2010.2107.

17 Hu, L., Song, J., Yin, X., Su, Z., & Li, Z. (2020). Research progress on polymer solar cells based on PEDOT: PSS electrodes, *Polymers*, 12(1), 145. https://doi.org/10.3390/polym12010145.

18 Xia, Y., & Dai, S. (2021). Review on applications of PEDOTs and PEDOT: PSS in perovskite solar cells, *Journal of Materials Science: Materials in Electronics*, 32, 12746-12757. https://doi.org/10.1007/s10854-020-03473-w.

19 Yang, Y., Deng, H., & Fu, Q. (2020). Recent progress on PEDOT: PSS based polymer blends and composites for flexible electronics and thermoelectric devices, *Materials Chemistry Frontiers*, 4, 3130-3152. https://doi.org/10.1039/d0qm00308e.

20 Aimukhanov, A.K., Rozhkova, X.S., Ilyassov, B.R., Zeinidenov, A.K., & Nuraje, N. (2021). The influence of structural and charge transport properties of PEDOT: PSS layers on the photovoltaic properties of polymer solar cells, *Polymers for Advanced Technologies*, 32(2), 497-504. https://doi.org/10.1002/pat.5102.

21 Rozhkova, X.S., Aimukhanov, A.K., Ilyassov, B.R., & Zeinidenov, A.K. (2022). The role of alcoholic solvents in PEDOT: PSS modification as hole transport layers for polymer solar cells, *Optical Materials*, 131, 112708. https://doi.org/10.1016/j.optmat.2022.112708.

22 Aimukhanov, A.K., Rozhkova, X.S., Zeinidenov, A.K., & Seisembekova, T.E. (2021). Influence of surface structure and morphology of PEDOT: PSS on its optical and electrophysical characteristics, *Bulletin of the University of Karaganda-Physics,* 103(3), 93-100. https://doi.org/10.31489/2021ph3/93-100.

23 Aimukhanov, A., Rozhkova, X., Ilyassov, B., Omarbekova, G., & Seisembekova, T. (2022). Effect of alcohol solvents on the structural, optical and electrical characteristics of PEDOT: PSS polymer films annealed at low atmospheric pressure, *Eurasian Physical Technical Journal*, 19, 2(40), 35-41. https://doi.org/10.31489/2022No2/35-41.

24 Rozhkova, X.S., Aimukhanov, A.K., Zeinidenov, A.K., & Alexeev A.M. (2022). Influence of the environment on the morphology, optical and electrical characteristics of the PEDOT: PSS polymer, *Bulletin of the University of Karaganda-Physics,* 106(2), 117-126. https://doi.org/10.31489/2022Ph1/117-126.

25 Nguyen, E.P., Carey, B.J., Daeneke, T., Ou, J.Z., Latham, K., Zhuiykov, S., & Kalantar-Zadeh, K. (2015). Investigation of two-solvent grinding-assisted liquid phase exfoliation of layered MoS₂, *Chemistry of Materials*, 27(1), 53-59. https://doi.org/10.1021/cm502915f.

26 Chhowalla, M., Shin, H.S., Eda, G., Li, L.J., Loh, K.P., & Zhang, H. (2013). The chemistry of two dimensional layered transition metal dichalcogenide nanosheets, *Nature Chemistry*, 5, 263-275. https://doi.org/10.1038/nchem.1589.

27 Chang, J., Register, L.F., & Banerjee, S.K. (2013). Atomistic Full-band simulations of monolayer MoS₂ transistors, *Applied Physics Letters*, 103(22), 10451-10453. https://doi.org/10.1063/1.4837455.

28 Anrango-Camacho, C., Pavón-Ipiales, K., Frontana-Uribe, B.A., & Palma-Cando, A. (2022). Recent advances in hole-transporting layers for organic solar cells, *Nanomaterials*, 12(3), 443. https://doi.org/10.3390/nano12030443.

29 Cheng, R., Li, D., Zhou, H., Wang, C., Yin, A., Jiang, S., Liu, Y., Chen, Y., Huang, Y., & Duan, X. (2014). Electroluminescence and photocurrent generation from atomically sharp WSe₂/MoS₂ heterojunction p–n diodes, *Nano Letters*, 14(10), 5590-5597. https://doi.org/10.1021/nl502075n.

30 Lin, Y., Adilbekova, B., Firdaus, Y., Yengel, E., Faber, H., Sajjad, M., Zheng, X., Yarali, E., Seitkhan, A., Bakr, O.M., El-Labban, A., Schwingenschlogl, U., Tung, V., McCulloch, I., Laquai, F., & Anthopoulos, T.D. (2019). 17 % efficient organic solar cells based on liquid exfoliated WS₂ as a replacement for PEDOT: PSS, *Advanced Materials*, 31(46), 1902965. https://doi.org/10.1002/adma.201902965.

31 Chang, J., Register, L.F., & Banerjee, S.K. (2013). Atomistic Full-band simulations of monolayer MoS₂ transistors, *Applied Physics Letters*, 103, 223509. https://doi.org/10.1063/1.4837455.

32 Kim, K., Ihm, K. & Kim, B. (2015). Surface property of indium tin oxide (ITO) after various methods of cleaning, *Acta Physica Polonica A*, 127(4), 1176-1179. https://doi.org/10.12693/APhysPolA.127.1176.

33 Dong, N., Li, Y., Feng, Y., Zhang, S., Zhang, X., Chang, C., Fan, J., Zhang, L., & Wang, J. (2015). Optical limiting and theoretical modelling of layered transition metal dichalcogenide nanosheets, *Scientific Reports*, 5, 14646. https://doi.org/10.1038/srep14646.

34 Coleman, J.N., Lotya, M., O'neill, A., Bergin, S.D., King, P.J., Khan, U., Young, K., Gaucher, A., De, S., Smith, R.J., Shvets, I.V., Arora, S.K., Stanton, G., Kim, H.-Y., Lee, K., Kim, G.T., Duesberg, G.S., Hallam, T., Boland, J.J., Wang, J.J., Donegan, J.F., Grunlan, J.C., Moriarty, G., Shmeliov, A., Nicholls, R.J., Perkins, J.M., Grieveson, E.M., Theuwissen, K., Mccomb, D.W., Nellist, P.D., & Nicolosi, V. (2011). Two-dimensional nanosheets produced by liquid exfoliation of layered materials, *Science*, 331(6017), 568-571. https://doi.org/10.1126/science.119497.

35 Liu, H.-L., Shen, C.-C., Su, S.-H., Hsu, C.-L., Li, M.-Y., & Li, L.-J. (2014). Optical properties of monolayer transition metal dichalcogenides probed by spectroscopic ellipsometry. *Applied Physics Letters*, 105(20), 201905. https://doi.org/10.1063/1.4901836.

36 Eda, G., & Maier, S. A. (2013). Two-dimensional crystals: managing light for optoelectronics. *ACS Nano*, 7(7), 5660-5665. https://doi.org/10.1021/nn403159y.

37 Xia, Y., Sun, K., & Ouyang, J. (2012). Highly conductive poly(3,-4-ethylenedioxythiophene): poly(styrene sulfonate) films treated with an amphiphilic fluoro compound as the transparent electrode of polymer solar cells, *Energy & Environmental Science*, 5, 5325-5332. https://doi.org/10.1039/C1EE02475B.

38 Yuan, X., Song, C., Wang, H., & Zhang, J. (2010). EIS Equivalent Circuits in Electrochemical Impedance Spectroscopy in PEM Fuel Cells. *Springer-Verlag,* London, England, 420p. https://doi.org/10.1007/978-1-84882-846-9.

39 Khanam, J.J., & Foo, S.Y. (2019). Modeling of high-efficiency multi-junction polymer and hybrid solar cells to absorb infrared light, *Polymers*, 11(2), 383. https://doi.org/10.3390/polym11020383.

40 Xing, W., Chen, Y., Wu, X., Xu, X., Ye, P., Zhu, T., Guo, Q., Yang, L., Li, W., & Huang, H. (2017). PEDOT: PSS-assisted exfoliation and functionalization of 2D nanosheets for high-performance organic solar cells, *Advanced Functional Materials*, 27(32), 1701622. https://doi.org/10.1002/adfm.201701622.

К.С. Рожкова, А.К. Аймуханов, Б.Р. Ильясов, А.К. Тусупбекова,
А.К. Зейниденов, А.М. Алексеев, А.М. Жаканова

WS$_2$ нанобөлшектерінің полимерлі күн элементінің вольт-амперлік сипаттамаларына әсері

WS$_2$ нанобөлшектерінің PEDOT: PSS полимерлі күн элементінің оптикалық және электр тасымалдау сипаттамаларына әсері туралы зерттеу нәтижелері келтірілген. WS$_2$ нанобөлшектері изопропил спиртіндегі лазерлік абляция әдісімен алынды. Нанобөлшектердің орташа өлшемдері жарықтың динамикалық шашырау әдісімен анықталды және ~ 38 нм құрады. Ерітіндідегі WS$_2$ нанобөлшектерінің концентрациясын есептеу WS$_2$ затының тығыздығына негізделген. Изопропил спиртіндегі нанобөлшектердің жұтылу спектрі өлшенді. Жұтылу спектрінде 500-900 нм аймағында байқалған екі максимум 2H фазасындағы екі өлшемді өтпелі металл дихалькогенидтерінің A1 және B1 түзу экситондық ауысуларымен байланысты. WS$_2$ нанобөлшектері қабыршақтүзетін ерітінді дайындау сатысында PEDOT: PSS-ке легирленген. АКМ суреттері бойынша бағаланатын бетінің R_a орташа арифметикалық ауытқу параметрі анықталды. WS$_2$ нанобөлшектерін қосу қабыршақтың R_a параметрінің артуына алып келеді. Нанокомпозиттік қабыршақтардың оптикалық жұтылу спектрлері өлшенді. WS$_2$ нанобөлшектерін PEDOT: PSS-ке легирленген кезде PEDOT жұтылу максимумының ұзын толқынды ығысуы байқалады. Қабыршақ кедергісі шамамен 2 есе азаятын, заряд тасушылардың рекомбинациялық кедергісі 4,7 есе артатын, ал полимерлі күн батареясының тиімділігі 1,94 % дейін артатын PEDOT: PSS: NP WS$_2$ нанокомпозиттік қабыршағының құрамындағы WS$_2$ нанобөлшектерінің критикалық концентрациясы анықталды.

Кілт сөздер: PEDOT: PSS, WS$_2$ нанобөлшектер, кемтікті-тасымалдаушы қабат, беттік морфология, жұтылу спектрлері, импеданс спектроскопиясы, органикалық күн ұяшығы, вольт-амперлік сипаттамалары.

К.С. Рожкова, А.К. Аймуханов, Б.Р. Ильясов, А.К. Тусупбекова,
А.К. Зейниденов, А.М. Алексеев, А.М. Жаканова

Влияние наночастиц WS$_2$ на вольт-амперные характеристики полимерного солнечного элемента

Представлены результаты исследований влияния наночастиц WS$_2$ на оптические и электротранспортные характеристики PEDOT: PSS полимерного солнечного элемента. Наночастицы WS$_2$ были получены методом лазерной абляции в изопропиловом спирте. Средние размеры наночастиц были определены методом динамического рассеяния света и составили ~ 38 нм. Расчет концентрации наночастиц WS$_2$ в растворе производился, исходя из плотности вещества WS$_2$. Измерен спектр поглощения наночастиц в изопропиловом спирте. Наблюдаемые два максимума в спектре поглощения в области 500–900 нм связаны с прямыми экситонными переходами A1 и B1 двумерных дихалькогенидов переходных металлов в 2H-фазе. Наночастицы WS2 были легированы в PEDOT: PSS на стадии приготовления пленкообразующего раствора. По АСМ снимкам был определен параметр среднеарифметического отклонения оцениваемой поверхности R_a. Допирование наночастицами WS$_2$ приводит к изменению R_a пленки в сторону возрастания. Измерены спектры оптического поглощения нанокомпозитных пленок. Показано, что при легировании наночастиц WS2 в PEDOT: PSS наблюдается длинноволновый сдвиг максимума поглощения PEDOT. Определена критическая концентрация наночастиц WS$_2$ в составе нанокомпозитной пленки PEDOT: PSS: NP WS$_2$, при которой сопротивление пленки уменьшается почти в 2 раза, рекомбинационное сопротивление носителей заряда возрастает в 4,7 раза, а эффективность полимерного солнечного элемента увеличивается до 1,94 %.

Ключевые слова: PEDOT: PSS, наночастицы WS$_2$, дырочно-транспортный слой, морфология поверхности, спектры поглощения, импедансная спектроскопия, органическая солнечная ячейка, вольт-амперные характеристики.